Temperature-correlated Afterglow of Semiconducting Polymer Nanococktail for Imaging-Guided Photothermal Therapy

Xu Zhen, Chen Xie, and Kanyi Pu*

Abstract: Real-time temperature monitoring is critical to reduce the nonspecific damage during photothermal therapy (PTT); however, PTT agents that can emit temperature-related signals are rare and limited to few inorganic nanoparticles. We herein synthesize semiconducting polymer nanococktail (SPN_{CT}) that can not only convert photo-energy to heat but also emit temperature-correlated luminescence after cessation of light excitation. Such an afterglow luminescence of SPN_{CT} detects tumor more sensitively than fluorescence due to the elimination of tissue autofluorescence, while its temperature-dependent nature allows to optically monitor tumor temperature under near-infrared (NIR) laser irradiation. Thus, SPN_{CT} represents the first organic optical nanosystem that enables optical imaging guided PTT without real-time light excitation.

Photothermal therapy (PTT) capitalizes on light-absorbing materials to generate hyperthermia under near-infrared (NIR) laser irradiation, provides new opportunities for cancer therapy.[1] However, the requirement of heating tumor tissue above 45°C or even higher for effective cancer ablation poses the potential risk to damage surrounding normal tissues.[2] To improve the therapeutic efficiency and reduce side effect in cancer therapy, temperature constitutes a critical factor that needs to be precisely monitored during PTT.

One emerging strategy to monitor the temperature during PTT lies in the utilization of temperature-sensitive optical agents.[3] However, agents that can change their fluorescence intensity, spectral profile, or fluorescence lifetime in response to temperate are rare.[4] Until now, only PbS/CdS/ZnS quantum dots (QDs) and lanthanide-based upconversion nanoparticles have been revealed to have such ability for real-time monitoring of temperature during PTT.[5] However, both fluorescence and up-conversion luminescence require real-time light excitation, which not only interferes the photothermal irradiation light but also compromises the imaging sensitivity due to tissue autofluorescence. Moreover, organic nanoparticles with intrinsic heat-reporting ability have not been reported for real-time temperature monitoring during PTT.

Semiconducting polymer nanoparticles (SPNs) are a new class of organic photonic nanomaterials made from optically-active semiconducting polymers (SPs).[6] As SPNs are completely organic, they avoid the potential issue of metal-ion induced toxicity and have been proven to generally possess good biocompatibility.[7] The structural versatility and excellent optical properties of SPNs have enabled a variety of imaging applications including fluorescence,[8] chemiluminescence,[9] photoacoustic[10] or photothermal control[11]. Recently, we found that poly(phenylenevinylene) (PPV) derivatives could continuously emit light even after removal of light excitation.[12] Such an afterglow luminescence avoids the tissue autofluorescence, offering a signal-to-background ratio (SBR, the mean luminescence intensity in the signal region divided by the mean luminescence intensity of the normal tissue background) that is significantly higher than fluorescence imaging.

In this study, we report the design and synthesis of semiconducting polymer nanococktail (SPN_{CT}) with temperature-correlated afterglow luminescence for imaging-guided PTT. SPN_{CT} comprises two major components (**Figure 1**): an amphiphilic poly(ethylene glycol) (PEG) grafted PPV (PPV-PEG) and a near-infrared (NIR) absorbing poly(silolodithiophene-*alt*-diketopyrrolopyrrole (PCSD) serving as the temperature-monitoring sensor and photothermal agent, respectively. The hydrophobic PCSD polymer interacted with the hydrophobic backbone of PEG-PPV to form the nanoparticles with PEG chains covered on the surface. Such a multicomponent structure is defined as nanococktail. The temperature sensitivity is an intrinsic characteristic of the afterglow from PPVs, because the photon-releasing decomposition of dioxetane units within PPV is thermodynamically controlled (**Figure 1**).[12] PCSD within SPN_{CT} has an electron-withdrawing structural unit (diketopyrrolopyrrole) and an electron-donating structural unit (silolodithiophene). Such a charge-transfer backbone favors nonradioactive deactivation and thus facilitates the generation of heat after light excitation. Afterglow-imaging guided PTT works as follows: after systemic administration of SPN_{CT}, afterglow imaging enables more sensitive detection of tumor in living mice relative to fluorescence imaging; upon NIR light irradiation, SPN_{CT} efficiently converts photon energy into heat, leading to increased temperature for PTT; during PTT, the temperature-correlated afterglow of SPN_{CT} induced by light pre-irradiation allows to monitor the photothermal temperature. Such an afterglow imaging guided PTT also avoids the interference between light excitation for fluorescence and laser irradiation, facilitating real-time temperature monitoring for PTT.

To synthesize PPV with PEG grafts, monomers 1 and 2 were co-polymerized at the molar ratio of 1 to give PPV-Br (**Figure 1**a). Then, PPV-Br was reacted with sodium azide to substitute bromide with azide, affording the azide functionalized PPV. The resulted azide functionalized PPV was reacted with propargyl end-PEG (M_n = 2000) (PEG-alkyne) *via* copper(I)-catalyzed alkyne-azide cycloaddition (CuAAC) reaction to obtain the final PEG grafted PPV (PPV-PEG) (**Figure 1**a). The conversion of bromide into azide was confirmed by proton nuclear magnetic resonance (^{1}H NMR) spectra (**Figure S1**, Supporting Information), which showed the complete shift of the resonance peak of $–CH_2Br$ (3.39 ppm) into the peak of $–CH_2N_3$ (3.24 ppm). The peaks of PPV backbone (7.51, 7.18, 5.35, 4.66, 4.07, 3.95, 3.87, 1.44-1.27 and 1.04-0.75 ppm) and the peak of the repeating

[*] Dr. X. Zhen, Dr. C. Xie, Prof. K. Pu
School of Chemical and Biomedical Engineering
Nanyang Technological University
Singapore, 637457 (Singapore)
E-mail: kypu@ntu.edu.sg

Supporting information and the ORCID identification number(s) for the author(s) of this article can be found under: https://doi.org/10.1002/anie.2017XXXXX

UNDER

unit of PEG (3.65 ppm) were detected by ^{1}H NMR, confirming the structure of PPV-PEG (**Figure S2**, Supporting Information).

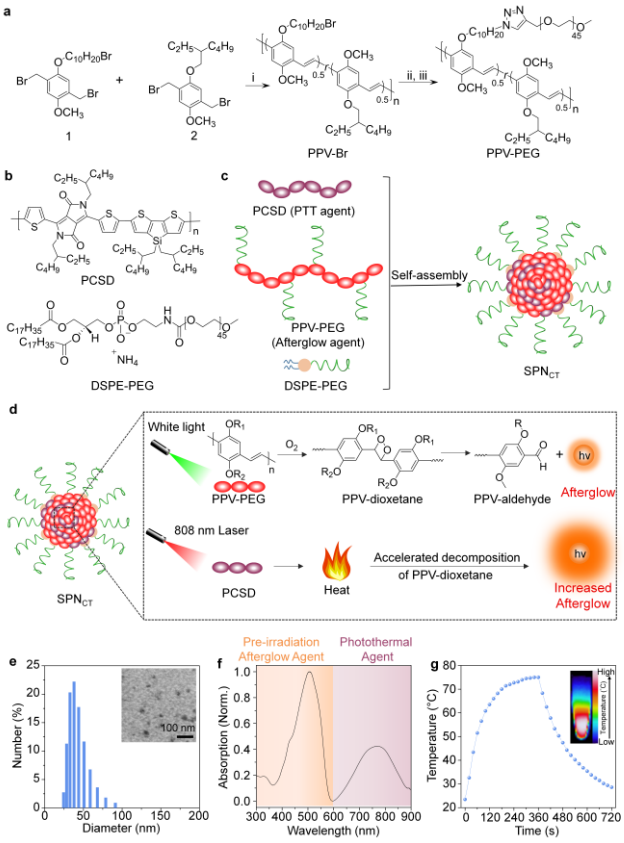

Figure 1. Synthesis and characterization of semiconducting polymer nanococktail (SPN_{CT}). (a) Synthetic routes of PPV-PEG. Reagents and conditions: (i) potassium tert-butoxide, tetrahydrofuran (THF), 25°C, overnight. (ii) sodium azide, THF/*N,N*-dimethylformamide (DMF), 40 °C, overnight. (iii) CuBr, *N,N,N',N'',N'''*-pentamethyldiethylenetriamine (PMDETA), PEG-alkyne, THF, 25 °C, 48 h. (b) Chemical structures of PCSD and DSPE-PEG. (c) Schematic illustration of the preparation of SPN_{CT} *via* nano-coprecipitation. (d) Schematic illustration of the mechanism for the photothermally-enhanced afterglow luminescence of SPN_{CT}. (e) Representative DLS profiles of SPN_{CT}. Inset: representative TEM image of SPN_{CT}. (f) Absorption spectra of SPN_{CT}. (g) The temperature of SPN_{CT} as a function of laser irradiating time. Inset: Thermal image of SPN_{CT} at its maximum temperature. The concentration of SPN_{CT} was 15 μg mL^{-1} based on the concentration of PCSD in 1× PBS (pH = 7.4). The laser irradiation wavelength was at 808 nm with a power of 1 W cm^{-2}.

The nanococktail (SPN_{CT}) was synthesized *via* nano-coprecipitation of PPV-PEG, PCSD, and 1,2-distearoyl-sn-glycero-3-phosphoethanolamine -poly(ethylene glycol)2000 (DSPE-PEG) (**Figure 1**b,c). PCSD was chosen as the photothermal agent (**Figure 1**b), which had the strong absorption of NIR light, while DSPE-PEG was used to further stabilize the nanoparticles. The doping amount was optimized to be 150 $_{w/w}$ % (PSCD: PPV-PEG), wherein the nanoparticles had the highest amount of PSCD but maintaining the stability (**Figure S3**, Supporting Information). Dynamic light scattering (DLS) showed that the SPN_{CT} had a relatively narrow size distribution with an average hydrodynamic diameter of ~40 nm (**Figure 1**e), and transmission electron microscopy (TEM) revealed the spherical morphology of SPN_{CT} (**Figure 1**e, inset). No precipitation and change in size were observed for SPN_{CT} after storage for 30 days, demonstrating the excellent stability in aqueous medium (**Figure S4**, Supporting Information).

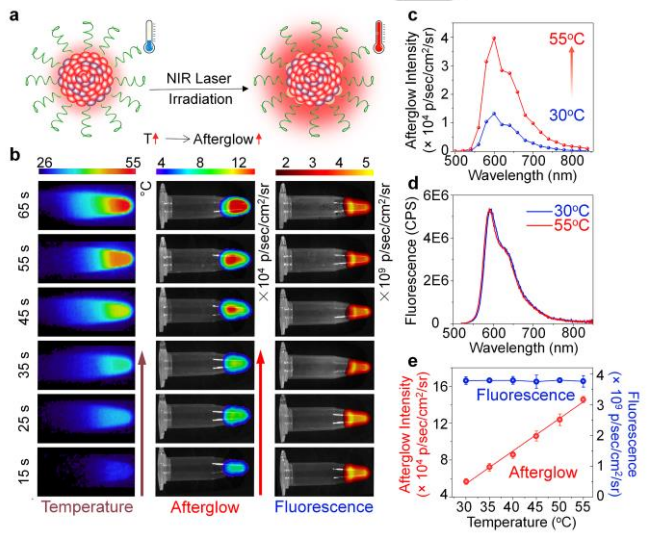

Figure 2. In vitro studies of photothermally-enhanced afterglow. (a) Schematic illustration of photothermally-enhanced afterglow luminescence of SPN_{CT}. (b) Temperature, afterglow and fluorescence images of SPN_{CT} (15 μg mL^{-1} based on the concentration of PCSD, 100 μL). in 1 × PBS buffer (pH = 7.4). SPN_{CT} was irradiated by white light (0.1 W cm^{-2}) for 1 min and simultaneously irradiated with laser at 808 nm (1 W cm^{-2}) for different amounts of time (15, 25, 35, 45, 55, or 65 s) to reach different temperatures (30, 35, 40, 45, 50, or 55 ºC). Note that the while-light irradiation was started 1 min before the end of NIR light irradiation. (c,d) Afterglow luminescence (c) and fluorescence spectra (d) of SPN_{CT} at 30 and 55 °C in 1 × PBS buffer (pH = 7.4). (e) Afterglow luminescence and fluorescence intensities as a function of the temperature of SPN_{CT}. Afterglow luminescence images were acquired for 10 s after irradiation by white light (0.1 W cm^{-2}) for 1 min. Fluorescence images were acquired for 0.1 s at 600 ± 10 nm upon excitation at 500 ± 10 nm.

The optical and photothermal properties of SPN_{CT} were studied in phosphate buffered saline (PBS) (pH = 7.4). SPN_{CT} had two absorption peaks with the maxima at 509 and 770 nm, respectively (**Figure 1**f). The peak at 509 nm was contributed from PPV-PEG, which was used to induce afterglow luminescence after cessation of light irradiation. The peak at 770 nm was assigned to PCSD, which allowed NIR photothermal heating. The peak mass extinction coefficients of PPV and PCSD were 63 and 72 cm^{-1} mg^{-1} mL, respectively. SPN_{CT} exhibited a fluorescence spectrum ranging from 550 to 750 nm with the maximum at 590 nm (**Figure S5**, Supporting Information). The afterglow luminescence of SPN_{CT} was detected without real-time excitation after preirradiation with white light (0.1 W cm^{-2}) for 1 min. SPN_{CT} showed strong afterglow luminescence and its spectrum was almost identical to the fluorescence spectrum with the emission maximum at 600 nm. (**Figure S5**, Supporting Information). Under continuous laser irradiation at 808 nm, SPN_{CT} showed gradually increased solution temperatures and reached plateau at t = 360 s (**Figure 1**g). The maximum photothermal temperature of SPN_{CT} was 75 °C and its photothermal conversion efficiency at 808 nm was calculated to be 35%. The reversible

heating-cooling operation showed that the maximum temperatures of SPN_{CT} remained nearly the same for at least 5 cycles, proving the good photothermal stability (**Figure S6**, Supporting Information).

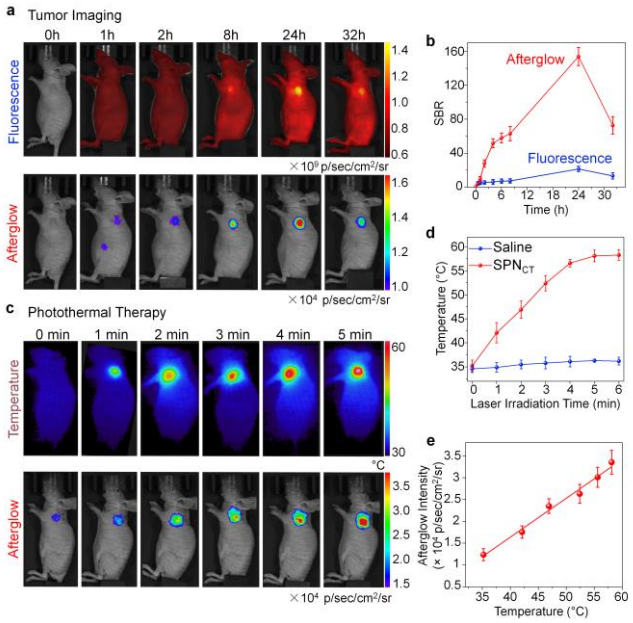

Figure 3. *In vivo* tumor imaging and afterglow-guided PTT. (a) Fluorescence and afterglow luminescence images of 4T1 tumor-bearing living mice at different time points after intravenous injection of SPN_{CT} (300 μg mL^{-1} based on the concentration of PCSD, 200 μL). (b) SBRs for fluorescence and afterglow imaging of tumor in living mice treated with SPN_{CT} as a function of post-injection time. (c) Thermal and afterglow images of tumor in living mice at 24 h after intravenous injection of SPN_{CT} under laser irradiation at 808 nm for different times with a power of 0.3 W cm^{-2}. (d) Mean tumor temperature during laser irradiation after intravenous injection of saline or SPN_{CT} into 4T1 tumor-bearing living mice at post injection time of 24 h. Error bars were based on standard error of mean (SEM) (n = 4). Laser irradiation at 808 nm with a power of 0.3 W cm^{-2}. (e) Quantification of *in vivo* afterglow luminescence of tumor as a function of photothermal temperature. Afterglow luminescence images were acquired for 10 s with an open filter after irradiation with white light (0.1 W cm^{-2}) for 1 min. Fluorescence images were acquired for 0.1 s at 600 ± 10 nm upon excitation at 500 ± 10 nm.

To study photothermally-enhanced afterglow, NIR laser and white-light irradiation were used to induce photothermal heating and afterglow of SPN_{CT}, respectively. The images were acquired immediately after NIR laser and white-light irradiation with the time gap of 2-3 s. With NIR laser irradiation, the temperature of SPN_{CT} solution was gradually increased (**Figure 2**a,b), resulting in increased afterglow intensity (**Figure 2**b). This was caused by the accelerated decomposition of the unstable PPV-dioxetane intermediate to PPV-aldehyde and photons.[12] The afterglow intensity was increased by 3.0-fold upon photothermal heating of the solution from 30 to 55 °C (**Figure 2**c). However, the fluorescence intensity remained the same regardless of the solution temperature (**Figure 2**b,d). A good linearity between temperature and afterglow signals of SPN_{CT} was observed (**Figure 2**e), showing its potential to quantify the temperature and thus guide PTT. The afterglow of SPN_{CT} decayed with a half-life of 4.5 min at room temperature (**Figure S7**, Supporting Information). The afterglow of SPN_{CT} could be repeatedly induced by white-light irradiation and no signal loss was observed under NIR laser multi-cycle heating. The optical spectra remained nearly the same, demonstrating the good photostability of SPN_{CT} (**Figure S8**, Supporting Information).

To examine PTT efficacy of SPN_{CT} *in vitro*, 4T1 cells were incubated with SPN_{CT} for 12 h and then irradiated for 5 min at 808 nm (0.5 W cm^{-2}). The cell status was qualitatively evaluated by calcein AM (live cells, green fluorescence) and propidium iodide (dead cells, red fluorescence) staining (**Figure S9**, Supporting Information) and also quantitatively measured by using 3-(4,5-dimethylthiazol-2-yl)-5-(3-carboxymethoxyphenyl)-2-(4-sulfophenyl)-2H-tetrazolium (MTS) assays (**Figure S10**, Supporting Information). SPN_{CT} had no obvious cytotoxicity in the absence of laser irradiation (**Figure S9**&**S10**, Supporting Information), demonstrating the good cytocompatibility. In contrast, almost all the cells were ablated by SPN_{CT} after laser irradiation, indicating the high PTT efficacy of SPN_{CT}.

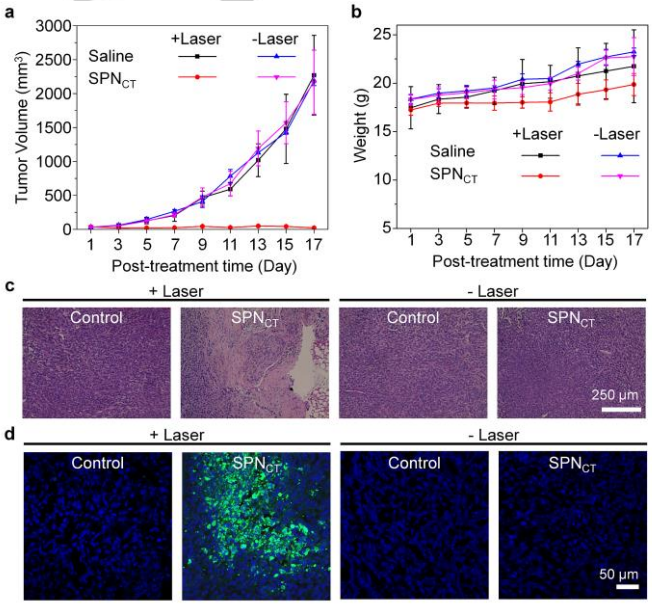

Figure 4. Evaluation of anti-tumor efficacy for afterglow-guided PTT. (a) Tumor growth curves and (b) body weight data of mice after intravenous injection of saline or SPN_{CT} with or without laser irradiation at 808 nm (n = 4). Error bars indicated standard error of mean (SEM) (n = 4). (c) H&E staining for tumors of mice treated with saline or SPN_{CT} with or without laser irradiation. (d) Immunofluorescent staining of caspase-3 for tumors on mice treated with saline or SPN_{CT} with or without laser irradiation. Green fluorescence indicates staining of caspase-3, while blue fluorescence indicates nucleus staining. All the treatments were done 24 h after intravenous injection of saline or SPN_{CT}. The tumors for H&E staining and immunofluorescent staining of caspase-3 were collected after 17 days of treatment.

The ability of SPN_{CT} for afterglow imaging guided PTT was tested on xenograft 4T1 tumor mouse model. The temperature, afterglow luminescence, and fluorescence signals were first acquired in real time after intratumoral injection of SPN_{CT}. In accordance with the *in vitro* data, a good linear correlation between temperature and afterglow signal in tumor region was detected for SPN_{CT}, demonstrating the feasibility of afterglow

imaging guided PTT *in vivo* (**Figure S11**, Supporting Information). The afterglow luminescence of SPN_{CT} was then tested and compared with fluorescence for passively targeted imaging of tumor in living mice. Afterglow and fluorescence signals were longitudinally acquired in real time after systemic administration of SPN_{CT} through tail-vein injection. Both signals gradually increased over time and reached peak at 24 h post-injection, but the SBR of afterglow images was higher than that of fluorescence images at each time point (Figure 3a,b). At t = 24 h, the SBR of afterglow images was 154 ± 10, 7.3-fold higher than the fluorescence images (21 ± 3 (Figure 3b)). The significantly higher SBR for afterglow imaging was attributed to the eliminated tissue autofluorescence. Such a high SBR of afterglow allowed to clearly distinguish the tumor signal from the background noise at t = 1 h post-injection; in contrast, fluorescence imaging only could do so at t = 24 h post-injection. These results coincided with the *ex vivo* and *in vivo* tissue-penetration studies, showing the significantly higher tissue penetration and imaging sensitivity of afterglow over fluorescence (**Figure S12**, Supporting Information). The *ex vivo* biodistribution data further validated that SPN_{CT} had the highest uptake in tumor followed by liver, intestine, stomach, and other major organs (**Figure S13**, Supporting Information). Such a favorable accumulation in tumor was consistent with our previous observation, which should be due to the small size and stable nanostructure of semiconducting polymer brush based nanoparticles.[13]

According to the afterglow and fluorescence imaging results, SPN_{CT} had the highest accumulation in tumor at 24 h post-injection, and thus PTT was conducted at this time point. The 4T1-tumor bearing mice were irradiated at 808 nm (0.3 W cm^{-2}) for 6 min. The tumor temperature for SPN_{CT}-treated mice gradually increased and reached plateau after laser irradiation for 5 min (**Figures 3**c,d & **Figure S14**, Supporting Information), which was significantly higher than that for saline-treated mice at all time points. Meanwhile, afterglow luminescence of SPN_{CT} in tumor region was monitored during laser irradiation. With the increased photothermal temperature, the afterglow luminescence gradually enhanced. A good linearity between temperature and afterglow signal in tumor region was observed during PTT (**Figure 3**e). Therefore, this data confirmed that SPN_{CT} could not only convert photo energy to heat for PTT, but also emit temperature-dependent afterglow signals for temperature monitoring during PTT. Moreover, due to the higher tissue penetration and imaging sensitivity of the afterglow luminescence of SPN_{CT}, it had the potential to monitor the temperature in deep tissue (**Figure S 17&18**, Supporting Information).[14]

To further evaluate the antitumor effect for SPN_{CT}-based afterglow imaging guided PTT, tumor sizes for different treatment groups were continuously monitored every other day for 17 days after PTT. The tumor growth for SPN_{CT}-treated mice were successfully inhibited after laser irradiation, which was not for other control groups (saline-treated mice with or without laser irradiation, and SPN_{CT}-treated mice without laser irradiation) (**Figure 4**a & **Figure S15**, Supporting Information). Note that the irradiation dose was generally lower than the previous studies using other organic and inorganic nanoparticles (**Table S1**, Supporting Information). No significant weight loss of mice was observed throughout the whole experimental period **(Figure 4**b), and no noticeable histopathological damage was observed in livers, kidneys, and spleens for all groups after PTT (**Figure 4**c & **Figure S16**, Supporting Information), indicating the biosafety of SPN_{CT}. In contrast, typical nucleus dissociation (**Figure 4**c) and a large fraction of apoptotic cells (green fluorescence) (**Figure 4**d) were clearly detected for the tumor tissues of SPN_{CT}-treated mice after PTT. These data verified that SPN_{CT}-mediated PTT had a high and specific antitumor effect.

In summary, we have synthesized optically active SPs and made them into nanococktails for afterglow-imaging guided PTT. Such an organic nanoagents (SPN_{CT}) had a high photothermal conversion efficiency (35%), and emitted afterglow luminescence after cessation of light excitation. With a small size (40 nm) and PEGylated surface, SPN_{CT} passively targeted tumor in living mice, showing a highest accumulation in tumor rather than in liver. Due to the eliminated tissue autofluorescence, the afterglow of SPN_{CT} enabled delineation of tumor in a more sensitive and rapider way than fluorescence. Moreover, because the afterglow intensity had a good linear correlation with temperature, it allowed to monitor the photothermal temperature of tumor under NIR laser irradiation. As a result of such ideal biophysical and photothermal properties along with its completely benign organic composition, SPN_{CT} permitted effective eradiation of tumor with a minimal damage to normal tissues in living mice. Thus, this study reports the first organic nanosystem that enables optical imaging guided PTT without real-time light excitation.

Acknowledgements

K.P. thanks Nanyang Technological University (Start-Up grant: NTUSUG: M4081627.120) and Singapore Ministry of Education (Academic Research Fund Tier 1: RG133/15 M4011559 and 2015-T1-002-091; and Tier 2 MOE2016-T2-1-098) for the financial support.

Conflict of interest

The authors declare no conflict of interest.

Keywords: semiconducting polymer nanococktail• afterglow-imaging guided photothermal therapy

[1] a) L. Cheng, C. Wang, L. Feng, K. Yang, Z. Liu, *Chem. Rev.* **2014**, *114*, 10869-10939; b) X. Huang, I. H. El-Sayed, W. Qian, M. A. El-Sayed, *J. Am. Chem. Soc.* **2006**, *128*, 2115-2120; c) Q. Chen, L. Xu, C. Liang, C. Wang, R. Peng, Z. Liu, *Nat. Commun.* **2016**, *7*, 13193; d) W. Tao, X. Ji, X. Xu, M. Ariful Islam, Z. Li, S. Chen, P. E. Saw, H. Zhang, Z. Bharwani, Z. Guo, j. Shi, O. C. Farokhzad, *Angew. Chem. Int. Ed.* **2017**,*56,* 11896-11900; *Angew. Chem.* **2017**, *129,* 12058-12062.

[2] a) Y. Yang, W. Zhu, Z. Dong, Y. Chao, L. Xu, M. Chen, Z. Liu, *Adv. Mater.* **2017**, *29,* 1703588.; b) M. Koishi, S. i. Yokota, T. Mae, Y. Nishimura, S. Kanamori, N. Horii, K. Shibuya, K. Sasai, M. Hiraoka, *Clin. Cancer Res.* **2001**, *7*, 215-219; c) D. Yoo, H. Jeong, S. H. Noh, J. H. Lee, J. Cheon, *Angew. Chem. Int. Ed.* **2013**, *52*, 13047-13051; *Angew. Chem.* **2013**, *125,* 13285-13289.

[3] X.D. Wang, O. S. Wolfbeis, R. J. Meier, *Chem. Soc. Rev.* **2013**, *42*, 7834-7869.

[4] D. Jaque, F. Vetrone, *Nanoscale* **2012**, *4*, 4301-4326.

[5] a) B. del Rosal, E. Carrasco, F. Ren, A. Benayas, F. Vetrone, F. Sanz-Rodríguez, D. Ma, Á. Juarranz, D. Jaque, *Adv. Funct. Mater.* **2016**, *26*, 6060-6068; b) X. Zhu, W. Feng, J. Chang, Y.-W. Tan, J. Li, M. Chen, Y. Sun, F. Li, *Nat. Commun.* **2016**, *7*, 10437; c) E. C. Ximendes, W. Q. Santos, U. S. Rocha, U. K. Kagola, F. Sanz-Rodríguez, N. Fernández, A. d. S. Gouveia-Neto, D. Bravo, A. M. Domingo, B. del Rosal, C. D. Brites, L. D. Carlos, D. Jaque, C. Jacinto, *Nano Lett.* **2016**, *16*, 1695-1703; d) E. C. Ximendes, U. Rocha, T. O. Sales, N. Fernández, F. Sanz-Rodríguez, I. R. Martín, C. Jacinto, D. Jaque, *Adv. Funct. Mater.* **2017**, *27,* 1702249.

[6] a) L. Feng, C. Zhu, H. Yuan, L. Liu, F. Lv, S. Wang, *Chem. Soc. Rev.* **2013**, *42*, 6620-6633; b) C. Zhu, L. Liu, Q. Yang, F. Lv, S. Wang, *Chem. Rev.* **2012**, *112*, 4687-4735; c) C. Wu, S. J. Hansen, Q. Hou, J. Yu, M. Zeigler, Y. Jin, D. R. Burnham, J. D. McNeill, J. M. Olson, D. T. Chiu, *Angew. Chem. Int. Ed.* **2011**, *50*, 3430-3434; *Angew. Chem.* **2011**, *123,* 3492-3496. d) L. Wu, I.-C. Wu, C. C. DuFort, M. A. Carlson, X. Wu, L. Chen, C.-T. Kuo, Y.

Qin, J. Yu, S. R. Hingorani, D. T. Chiu, *J. Am. Chem. Soc.* **2017**, *139*, 6911-6918.

[7] a) K. Pu, A. J. Shuhendler, J. V. Jokerst, J. Mei, S. S. Gambhir, Z. Bao, J. Rao, *Nat. Nanotechnol.* **2014**, *9*, 233-239; b) K. Pu, A. J. Shuhendler, J. Rao, *Angew. Chem. Int. Ed.* **2013**, *52*, 10325-10329; *Angew. Chem.* **2013**, *125,* 10515-10519. c) K. Pu, N. Chattopadhyay, J. Rao, *J. Control. Release* **2016**, *240,* 312-322.

[8] G. Hong, Y. Zou, A. L. Antaris, S. Diao, D. Wu, K. Cheng, X. Zhang, C. Chen, B. Liu, Y. He, J. Z. Wu, J. Yuan, B. Zhang, Z. Tao, C. Fukunaga, H. Dai, *Nat. Commun.* **2014**, *5*, 4206.

[9] X. Zhen, C. Zhang, C. Xie, Q. Miao, K. L. Lim, K. Pu, *ACS Nano* **2016**, *10*, 6400-6409.

[10] a) Y. Lyu, X. Zhen, Y. Miao, K. Pu, *ACS Nano* **2016**, *11*, 358-367; b) X. Zhen, X. Feng, C. Xie, Y. Zheng, K. Pu, *Biomaterials* **2017**, *127*, 97-106.

[11] Y. Lyu, C. Xie, S. A. Chechetka, E. Miyako, K. Pu, *J. Am. Chem. Soc.* **2016**, *138*, 9049-9052.

[12] Q. Miao, C. Xie, X. Zhen, Y. Lyu, H. Duan, X. Liu, J. V. Jokerst, K. Pu, *Nat. Biotechnol.* **2017**, *35,* 1102.

[13] C. Xie, X. Zhen, Q. Lei, R. Ni, K. Pu, *Adv. Funct. Mater.* **2017**, *27,* 1605397.

[14] E. Carrasco, B. del Rosal, F. Sanz‐Rodríguez, Á. Juarranz, P. H. Gonzalez, U. Rocha, K. U. Kumar, C. Jacinto, J. G. Sole, D. Jaque, *Adv. Funct. Mater.* **2015**, 25, 615-626.

WILEY-VCH

Entry for the Table of Contents (Please choose one layout)

Layout 2:

COMMUNICATION

*Xu Zhen, Chen Xie, and Kanyi Pu**

Page No. – Page No.

Temperature-correlated Afterglow of Semiconducting Polymer Nanococktail for Imaging-Guided Photothermal Therapy

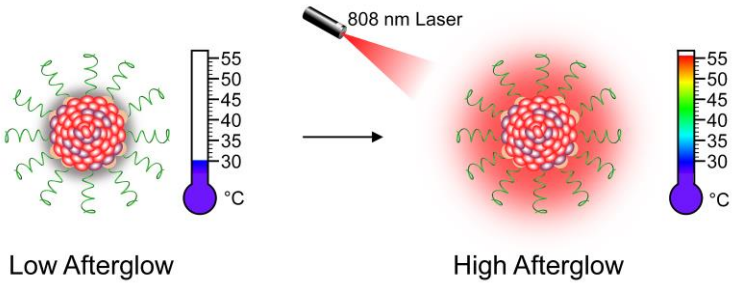

Afterglow imaging-guided photothermal therapy: Semiconducting polymer nanococktail (SPN_{CT}) with temperature-correlated afterglow luminescence is designed for imaging-guided photothermal therapy. The afterglow intensity of SPN_{CT} has a good linear correlation with temperature, allowing to monitor the photothermal temperature of tumor under NIR laser irradiation.

WILEY-VCH